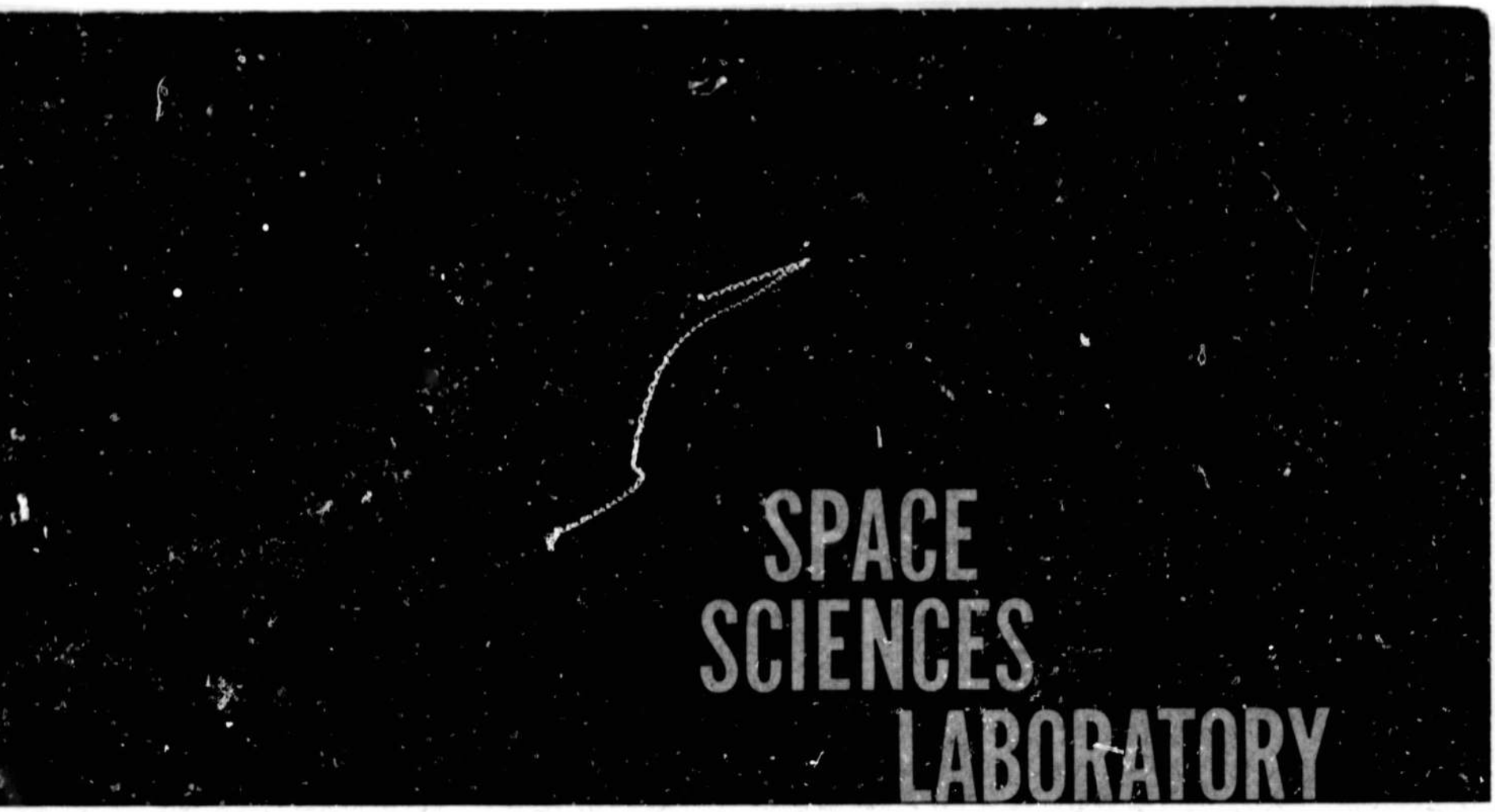


# SOLAR VELOCITY FIELDS: FIVE MINUTE OSCILLATIONS AND SUPERGRANULATION

Andrew S. Tanenbaum, John M. Wilcox,
Edward N. Frazier and Robert Howard



May 2, 1969
Series 10, Issue 16

UNIVERSITY OF CALIFORNIA, BERKELEY

# SOLAR VELOCITY FIELDS: FIVE MINUTE OSCILLATIONS AND SUPERGRANULATION*

Andrew S. Tanenbaum, John M. Wilcox,
Edward N. Frazier and Robert Howard

Technical Report

ONR Contract Nonr 3656(26), Project NR 021 101
Partial support from NASA Grant NGR 05-003-230,
NsG 243, and NSF Grant GA-1319



*Submitted to Solar Physics

# Solar Velocity Fields: Five Minute Oscillations and Supergranulation

Andrew S. Tanenbaum

John M. Wilcox, Edward N. Frazier*,

Space Sciences Laboratory

University of California

Berkeley, California 94720

and

Robert Howard

Mount Wilson and Palomar Observatories

Carnegie Institution of Washington

California Institute of Technology

Pasadena, California 91106

Abstract. One dimensional magnetograph scans have been used to study the five-minute photospheric velocity oscillations and the supergranulation. The oscillations in wing brightness lead the oscillations in velocity by less than 90° in the photosphere, and about 90° in the chromosphere, suggesting that they are traveling waves at lower levels and standing waves at higher levels. Downward flows have been observed to be coincident with the chromospheric network confirming the hypothesis that material is flowing downward at supergranular boundaries.

*Present address: Space Physics Laboratory, Aerospace Corporation, P. O. Box 95085, Los Angeles, California 90045.

## I. Introduction

Using an ingenious variation of the traditional spectroheliograph, LEIGHTON et al. (1962) discovered vertical velocity oscillations in the solar photosphere superimposed upon a system of horizontal flows which they designated the "supergranulation." Despite the fact that these motions have subsequently been investigated by numerous observers (e. g. EVANS and MICHARD, 1962c; NOYES and LEIGHTON, 1963; SIMON and LEIGHTON, 1964; DEUBNER, 1967; HOWARD, 1967; FRAZIER, 1968a; HOWARD, TANENBAUM and WILCOX ("Paper I"), 1968), using a variety of techniques (Leighton's method, spectra, magnetographs) there is still no generally accepted theory explaining either the nature of the oscillations, or the origin of the supergranulation. More observations are obviously needed. In this paper we shall continue the discussion of the five-minute oscillations and the supergranulation started in Paper I. That paper should be consulted for details of the equipment, observing techniques, and methods of data reduction.

## II. The Five-Minute Velocity Oscillations

Each observation consisted of a series of 300 one-dimensional scans back and forth along a line perpendicular to central meridian using the magnetographs at Mount Wilson Observatory and Kitt Peak National Observatory. We used apertures of 2.3, 2.4, 3.6, 5, and 10 arc seconds.

### A. Superposed Epoch Analysis

In order to study the five-minute oscillations in the wing brightness (e. g. EVANS et al., 1962; NOYES and LEIGHTON, 1963; JENSEN and ORRALL, 1963) a superposed epoch technique was used. After the reduction process described

in Paper I was applied to the Mount Wilson observations, it was possible to plot the velocity, as a function of time, for 200 separate points along the scan line (see Figure 5, Paper I). There was a residual drift in the velocity baseline of approximately $1.5 \times 10^{-3}$ Å/hour. We attribute this to a variation of the index of refraction of air (due to diurnal pressure changes) and perhaps to tower flexure (due to differential heating). This effect occurred almost every day, and was eliminated by passing each of the 200 velocity curves through a high pass frequency filter having a transmission of 99% at a period of 5 minutes and 50% at 17 minutes. The corresponding wing brightness was processed in precisely the same way, including the same high pass filtering to remove secant Z effects and other slow changes in the transparency.

Each velocity plot was then examined with the intent of determining the beginning and ending times of oscillating "wave trains." This cannot be done in any entirely satisfactory way, however, inasmuch as most "wave trains" have neither a well defined beginning nor a well defined end. The "start" of an oscillation was somewhat arbitrarily defined by an upward maximum of amplitude greater than 100 m/s. (Other discriminator levels were tried with no significant effects on the results.) This "start" was followed backward in time to the previous zero crossing, thus insuring that all "wave trains" had the same initial phase. Successive later extrema were examined until one smaller than 100 m/s was found. This defined the end of the "wave train" (see Figure 1).

This procedure was repeated for each of the 200 points along the scan line, giving a list of typically 600 separate "wave trains" for each day's observations. The velocity "wave trains" were then superposed to give one curve which can be regarded as an average velocity "wave train."

For each velocity "wave train" selected, the brightness observation at the same position and during the same time interval was selected. These brightness observations were then superposed to form a curve that might be regarded as the average brightness during a velocity "wave train." It is important to note that these brightness observations were chosen simply because the corresponding velocity observations were oscillatory; the shapes of the individual brightness curves used were not even examined.

Figures 2 and 3 show typical examples of the superposed epoch curves for velocity and for the corresponding wing brightness. The decrease of amplitude with time is at least partially due to oscillations of different periods getting out of phase. Therefore measurements of the period and phase are made on the first cycle of the superposed curves. Note that the amplitude of the brightness oscillation, $\triangle I/I$ is less than 1%. The velocity periods and brightness-velocity phase lags for four lines are shown in Table I. Using this technique we also found oscillations in the core brightness of Fe 5250.2, $K_{232}$ and even the continuum brightness, as shown in Figure 4. In every line investigated the brightness always led the velocity in the sense that maximum brightness occurred 30 to 80 seconds before maximum upward velocity.

Repeating this procedure, but substituting the velocity of another spectral line in place of the brightness channel of the magnetograph, we attempted to examine phase relations between lines formed at two different heights in the solar atmosphere. Comparisons were made between Na 5895.9 and a weak line Fe 5905.7. Comparisons were also made between Mg 5172.7 and another weak line Fe 5180.1. In all 4 runs examined the oscillations at the lower level definitely led the oscillations at the higher level. The average phase difference was 14 ± 3 seconds for the former pair, and 10 ± 3 seconds

for the latter pair. Since a sound wave would only propagate a distance of about 100 km in 14 seconds, and since this appears to be an unreasonably small separation between the heights of formation of these lines, we conclude that the vertical phase velocity is larger than the acoustic speed.

The brightness-velocity phase relations show a new and very interesting effect. In the wings of Na 5895.9 and Mg 5172.7 and the core of Fe 5250.2, the brightness leads the velocity by slightly more than $90^{\circ}$. This phase lead is consistent with the hypothesis that in the chromosphere the oscillations are standing adiabatic waves (c.f. NOYES and LEIGHTON, 1963; WHITNEY, 1958). The wing brightness in Fe 5250.2, the wing brightness in C 5380.3, and the continuum brightness all lead the velocity by significantly less than $90^{\circ}$. The brightness fluctuations observed in the wings of C 5380.3 and Fe 5250.2 probably are caused only by fluctuations in the continuum. If this is the case, then in order to compare brightness and velocity at the same level (i.e. the level of continuum formation), one must advance the velocity phase somewhat to account for the finite propagation time from the level of the continuum to the level of the line formation. Thus the phase lead of the brightness over the velocity is decreased even further. So we cannot avoid the fact that the brightness leads the velocity by less than $90^{\circ}$. This phase lead cannot be produced by standing waves of any type, either adiabatic or isothermal (WHITNEY, 1958). Thus we are led to the conclusion that the five-minute oscillations are traveling waves in the photosphere and standing waves in the chromosphere.

B. Fourier Analysis

These observations are particularly applicable to a two-dimensional Fourier analysis for two reasons: a) The large grid of both spatial points and temporal points over which the data is available means that a relatively large region in the k - $\omega$ plane may be investigated, and b) the large amount of data ensures statistical reliability of the results, an advantage that has been lacking in nearly all of the previous Fourier analyses.

The analysis procedure is identical to that described by FRAZIER (1968b). One wishes to compute the density of spectral power in the k - $\omega$ plane, where k is the horizontal wave number ($k = \sqrt{k_x^2 + k_y^2}$). This is done in a two step process. First, the autocorrelation is computed:

$$C(\lambda, \tau) = \langle\langle V(x, t)\, V(x + \lambda, t + \tau)\rangle_x\rangle_t$$

If we make the assumption that $C(\lambda, \tau)$ is azimuthally symmetric on the plane of the solar surface, then we can compute the power spectral density directly by making a combined Fourier transform over time and Hankel transform over space:

$$kF(k, \omega) = 4\pi\, k \int_0^\infty \lambda\, d\lambda \int_0^\infty d\tau\; C(\lambda, \tau)\, J_0(k\lambda) \cos(\omega\tau)$$

A contour plot is then made of $kF(k, \omega)$. Since this data was taken using magnetograph apertures of several different sizes (2".3, 3".6, and 5"), the power density was corrected for the transmission function of the aperture. It should be noted however that no correction was made for atmospheric seeing.

The region in the k - $\omega$ plane within which power can be observed is a function of the grid spacing and the maximum lag of the observations in x

and t. In all cases, the grid width in time was 40 seconds and the maximum lag was one hour, which means that periods between 80 seconds and 1/2 hour could be observed. The grid width in space varied from 1250 km to 5000 km and the maximum lag in space varied from 7500 km to 500,000 km. This means that wavelengths between 2500 km and 250,000 km were studied, though not necessarily in the same observation. A very important point to note is that although the smoothing effect of the finite magnetograph aperture has been corrected for, the seeing, which was only moderate at best, effectively filtered out all wavelengths shorter than approximately 6000 km. Observations of active regions were not used in this analysis.

The results can be seen in Figures 5 and 6. Each figure is a spectral density of a typical observation; they are reproducible both on succeeding days and on the two different magnetographs used (Mount Wilson and Kitt Peak). It should be pointed out that on each of the scans the very lowest wave numbers have been filtered out for numerical and instrumental reasons, so the decrease in power at the extreme left edge is spurious.

Several results are immediately obvious:

1) There is a large amount of power at very low frequencies and large wavelengths. This is the supergranulation that will be discussed in detail in section III.

2) The oscillatory power does not in general show the two frequencies that were observed by FRAZIER (1968b). The present analysis applies primarily for $\lambda \gtrsim 6000$ km, whereas the double frequencies were observed in the region $\lambda < 6000$ km. Figure 5 shows the single oscillatory "ridge" breaking up into two ridges at about $\lambda \approx 6000$ km, but the seeing has already filtered out the power so strongly that this feature must be considered marginally observed. It is however reproducible in the two separate Mount

Wilson scans and one Kitt Peak scan with this resolution. In conclusion, one can only say that there is definitely only one frequency at long wavelengths, and that more data is needed in the intermediate wavelength region (2000 km $\leq \lambda \leq$ 12000 km).

3) Figure 6 shows appreciable oscillatory power in a range of wavelengths from 6000 km out to 100,000 km or more. The power at long wavelengths could be caused by large, coherently oscillating regions, or alternatively it might be caused by the superposition of many smaller elements, oscillating randomly, sometimes in phase and sometimes out of phase. Below we present some evidence for the latter interpretation.

Consider an ensemble of N identical, independent oscillators of unit amplitude, constant frequency but random phase as a model for unresolved independently oscillating elements within the observer's aperture. He will see an average of all such elements, f,

$$f = \frac{1}{N} \sum_{i=1}^{N} \text{Sin } (\omega t + \phi_i)$$

The observed mean square velocity will be

$$f^2 = \frac{1}{N^2} \sum_{i=1}^{N} \sum_{j=1}^{N} \text{Sin } (\omega t + \phi_i) \text{ Sin } (\omega t + \phi_j)$$

The time average will be

$$\overline{f^2} = \frac{1}{N^2} \sum_{i=1}^{N} \sum_{j=1}^{N} \frac{1}{2} \text{ Cos } (\phi_i - \phi_j)$$

$$= \frac{1}{2N^2} \sum_{i=j} \text{ Cos } (\phi_i - \phi_j) + \frac{1}{2N^2} \sum_{i \neq j} \text{ Cos } (\phi_i - \phi_j)$$

$$= \frac{1}{2N} + \frac{1}{2N^2} \sum_{i \neq j} \text{ Cos } (\phi_i - \phi_j)$$

Taking an ensemble average the second term vanishes, giving a rms velocity equal to the value for a single oscillator (in this case $A^2/2$) divided by the square root of the number of independent oscillating elements. Since the number of elements seen grows linearly with the area of the observing aperture, we would expect the observed amplitude to decrease as the square root of the area, i.e. decrease in proportion to the radius of the aperture. This model can be tested by comparing previously published observed amplitudes with the aperture sizes that were used. Figure 7 shows this comparison. For aperture sizes greater than approximately 3000 km, the amplitude appears to decrease as expected.

To simulate the effect of still larger apertures the velocity was computed as a function of time not just at one point on the scan line, but averaged over several positions. This simulates an aperture which has been enlarged in one dimension only. The number of elements within the simulated aperture will then be proportional to its length, and the observed amplitude should decrease as the square root of the length. Figure 8 shows the rms velocity for simulated apertures of various lengths. The slope is close to -0.5 as would be expected from this model.

The presence of five-minute oscillations in observations of the 3 cm radio emission integrated over a large portion of the disk (YUDIN, 1968) might be taker as evidence that the scale size of the oscillating region is very large. The preceding discussion, however, suggests that some power may still be seen even though the observer integrates over many individual elements.

As a further check on the possible existence of very large oscillating regions, we computed the velocity as a function of time averaged over two separate large regions on the scan line: the eastern third and the western third. (The gap of 167,000 km between them insures observational independence.)

The five-minute oscillations were still detectable, as would be expected on the basis of Figure 8, but the phase between the two parts varied randomly from day to day, indicating no physical connection.

## III. The Supergranulation

Although it would be highly desirable to study the five-minute oscillations and the supergranulation by making two-dimensional raster scans with a magnetograph, this is quite difficult with existing equipment. In particular, it would be necessary to complete each raster in a time short compared to 5 minutes, lest the two velocity fields become hopelessly intertwined. For this reason, one-dimensional scans can still be useful, since each scan requires only a small fraction of 5 minutes (20 seconds in this case). We have averaged together 300 one-dimensional scans (i.e. at each position we averaged over several hours) to suppress the effects of the oscillatory field. Several examples are shown in Figure 9.

In each of the curves in Figure 9 one can see a series of downward velocity peaks spaced roughly 30,000 km apart. There is a similar series of upward velocity peaks interspersed with the downward ones. We propose to associate the downward peaks (corresponding to motion into the sun) with supergranular boundaries, and the upward peaks with the centers of supergranules. By superposing all 54 clear examples of downward and upward peaks (by aligning the minima or maxima) we get the composite curves of Figures 10a and 10b respectively. These are consistent with the above hypothesis. In particular, in Figure 10a the minimum is surrounded by two upward flows about 30,000 km apart, and in Figure 10b the maximum is likewise surrounded by downward flows. The difference between the amplitude of the upward peaks

Figure 10a and in Figure 10b is due to a spread in widths, so that in Figure 10 the maxima are not well aligned and the average is therefore smaller. There is no unambiguous way to select out all the peaks; in this case, only well isolated peaks were used. This will introduce a systematic uncertainty into the half widths. Furthermore, the scan line usually intersects a supergranule as a chord, not as a diameter. This causes the observed width to be less than the true width by a factor of $4/\pi$ if the supergranules were circular, and by other factors for other shapes.

Figure 11 shows a one-dimensional scan in which the brightness of the core of Fe 5250.2, of $K_{232}$, and of the vertical velocity in Fe 5233.0 were recorded simultaneously. In this figure one sees for the first time a good correlation between the downward velocity peaks and calcium emission, indicating that these downward peaks are in fact supergranular boundaries. In addition, it is clear that the photospheric network, as seen in the core of Fe 5250.2 and the chromospheric network, as seen in $K_{232}$ are coincident (D'AZAMBUJA, 1930; CHAPMAN and SHEELEY, 1968).

Figure 12 shows a comparison between the velocity averaged over $3^h\ 20^m$ as seen simultaneously in a chromospheric line Na 5895.9 and a photospheric line Fe 5905.7. The locations of the supergranular boundaries determined from the locations of the downward peaks are in good agreement, indicating that the supergranules persist over several hundred km in altitude. Observations made with Mg 5172.7 and Fe 5180.1 show a similar agreement.

Figure 13 shows a comparison between brightness in the wings of Fe 5250.2 and the magnetic field in a quiet region of the solar surface. Wherever there is an increase in field strength there is a brightening in the wings. This is probably the same phenomenon as Sheeley's "gaps"

(1967). Figure 14 is a scatter diagram of brightness variation versus field strength. There is a monotonic increase in brightness with absolute field magnitude.

## IV. Summary and Conclusions

1. The oscillations in wing brightness of C 5380.3, Fe 5250.2, Na 5895.9, and Mg 5172.7 lead the oscillations in the corresponding velocities. The amount of the phase shift increases with altitude, from less than 90° in the photosphere to approximately 90° in the low chromosphere. From this we conclude that the oscillations are traveling waves in the photosphere and standing adiabatic waves in the low chromosphere.

2. Fourier analysis reveals that the 300 second period does not resolve into two periods at spatial wavelengths $\geq$ 6000 km.

3. The observed amplitudes and sizes of the oscillations are consistent with a picture of many small oscillating elements superposing to give the appearance of larger ones. The oscillating elements appear on the average to be smaller than our effective resolution (6000 km).

4. Regions of downward flowing material have been observed, which correlate well with the boundaries of supergranular cells as defined by the chromospheric network. Upward flows usually occur near the middle of the cells. We conclude that the model of a supergranular cell proposed by LEIGHTON et al. (1962) is correct.

5. Patches of strong magnetic field (10 to 40 arc seconds in size) in quiet regions almost always are associated with brightenings in the wings of photospheric lines. The amount of brightening increases with increasing field strength.

## Acknowledgements

We would like to express our appreciation to the Kitt Peak National Observatory and Dr. W. C. Livingston for making available and operating the Kitt Peak magnetograph. We would also like to acknowledge the assistance of Mr. Philip Scherrer in reducing the Kitt Peak observations. This research was supported in part by the Office of Naval Research under contracts Nonr 3656(26) with the University of California and N00014-66-C-0239 with the Carnegie Institution of Washington, by the National Aeronautics and Space Administration under grants NsG 243 and NGR 05-003-230, and by the National Science Foundation under grant GA-1319.

## References

CHAPMAN, G. A. and SHEELEY, N. R.: 1968, Solar Phys. 5, 442.

D'AZAMBUJA, L.: 1930, Ann. Obs. Meudon 8, 22.

DEUBNER, F. L.: 1967, Solar Phys. 2, 133.

EDMONDS, F. N., JR., MICHARD, R. and SERVAJEAN, R.: 1965, Ann. d'Astrophys. 28, 534.

EVANS, J. W., MAIN, P., MICHARD, R. and SERVAJEAN, R.: 1962, Astrophys. J. 136, 682.

EVANS, J. W. and MICHARD, R.: 1962a, Astrophys. J. 135, 812; 1962b, Astrophys. J. 136, 487; 1962c, Astrophys. J. 136, 493.

FRAZIER, E. N.: 1968a, Astrophys. J. 152, 557.

FRAZIER, E. N.: 1968b, Z. Astrophys. 68, 345.

HOWARD, R.: 1967, Solar Phys. 2, 3.

HOWARD, R., TANENBAUM, A. S. and WILCOX, J. M.: 1968, Solar Phys. 4, 286.

JENSEN, E. and ORRALL, F. W.: 1963, Astrophys. J. 138, 252.

LEIGHTON, R. B., NOYES, R. W. and SIMON, G. W.: 1962, Astrophys. J. 135, 474.

LIVINGSTON, W. C.: 1968, Astrophys. J. 153, 929.

NOYES, R. W. and LEIGHTON, R. B.: 1963, Astrophys. J. 138, 631.

RODDIER, F.: 1966, Ann. d'Astrophys. 29, 639.

SHEELEY, N. R.: 1967, Solar Phys. 1, 171.

SIMON, G. W. and LEIGHTON, R. B.: 1964, Astrophys. J. 140, 1120.

WHITNEY, E.: 1958, Smithsonian Contr. Astrophys. 2, 365.

YUDIN, O. I.: 1968, Doklady Akademii Nauk SSR, Astronomia 180, 821.

## Figure Captions

Fig. 1. Schematic description of the method by which the oscillating "wave trains" are selected. The descriminator level of 100 m/s is indicated by the dashed line. Point A is the maximum which signals the beginning. Point B is actually used as the beginning, so that all "wave trains" will start in phase. Point C is the end of the "wave train."

Fig. 2. Superposed epoch curves for velocity and wing brightness in Fe 5250.2. Blue shifts (material flowing out of the sun) are shown as positive velocities in this and all subsequent figures. Observations made with a 5" aperture at Mount Wilson.

Fig. 3. Superposed epoch curves for velocity and wing brightness in Na 5895.9. Observations made with a 10" aperture at Mount Wilson.

Fig. 4. Superposed epoch curves for simultaneous measurements of velocity in Fe 5250.2, of wing brightness in Fe 5250.2, of core brightness in Fe 5250.2, of $K_{232}$, and of continuum brightness. All curves were synchronized with velocity in Fe 5250.2. Observations made with 2".4 aperture at Kitt Peak.

Fig. 5. Fourier transform of vertical velocities measured in Fe 5250.2. The two major components are the five-minute oscillations and the supergranulation. Observations made with 2".3 aperture at Mount Wilson.

Fig. 6. Same as Figure 5, but with a 5" aperture.

Fig. 7. The rms amplitude of the vertical velocity oscillations as a function of the aperture size used. Aperture size here is the length of a square aperture; cirucular apertures were reduced to square apertures of equivalent area. For observations that did not use an aperture, the effective resolution was plotted as the aperture size. For apertures larger than approximately 3000 km, the amplitude is inversely proportional to the aperture size.

Fig. 8. The rms amplitude of the vertical velocity oscillations as a function of the "simulated aperture length." The amplitude decreases as the square root of the aperture length. Observations made with a 5" aperture at Mount Wilson.

Fig. 9. Velocity as a function of position along the scan line. Each curve is an average of 300 scans. The top curve is for July 2, 1967 at 15°N. The bottom curve is for July 18, 1967 at 15°N. A 5" aperture was used for both observations, which were made at Mount Wilson.

Fig. 10. a) A composite of a supergranular boundary, made by superposing all 54 clear examples of downward peaks outside active regions. b) A composite of the center of a supergranule, made by superposing all 58 clear examples of upward peaks outside active regions. Observations made with a 5" aperture at Mount Wilson.

Fig. 11. The upper curve is the core brightness of Fe 5250.2, which shows the photospheric network. The middle curve is $K_{232}$. The lower curve is the

velocity measured in a photospheric iron line. Each curve is an average of 300 scans. Observations made at Kitt Peak on October 26, 1968 at the center of the visible disk with a 2".4 aperture.

Fig. 12. Velocity measured simultaneously in two lines, Na 5895.9 in the top curve, and a weak photospheric line Fe 5905.7 in the bottom curve. Each curve is an average of 300 scans. Observations made at Mount Wilson on August 19, 1967 at the center of the disk with a 10" aperture.

Fig. 13. Brightness in the wings of Fe 5250.2 measured simultaneously with the magnetic field in wings of Fe 5250.2. Each curve is an average of 300 scans. Observations made on July 15, 1967 at 15°N with a 5" aperture at Mount Wilson.

Fig. 14. Relation between field strength and brightness. Each point represents the field strength and brightness for a point on the scan line at which the field strength was a local maximum (of either polarity). Each circle represents the centroid of one tenth of the data. This was done by dividing the points into ten equal groups along the magnetic axis. Observations made throughout July 1967 at Mount Wilson with a 5" aperture.

TABLE I

Velocity Periods and Brightness-Velocity Phase

Lags from Superposed Epoch Method

| Spectral Line | Velocity Period (seconds) | Brightness-Velocity Phase lag (seconds) | Brightness-Velocity Phase Angle (degrees) |
|---|---|---|---|
| C 5380.3 | 306 ± 6 | 34 ± 13 | 40 ± 15 |
| Fe 5250.2 | 298 ± 2 | 52 ± 8 | 64 ± 10 |
| Na 5895.9 | 288 ± 6 | 78 ± 7 | 98 ± 8 |
| Mg 5172.7 | 280 ± 11 | 78 ± 5 | 100 ± 14 |

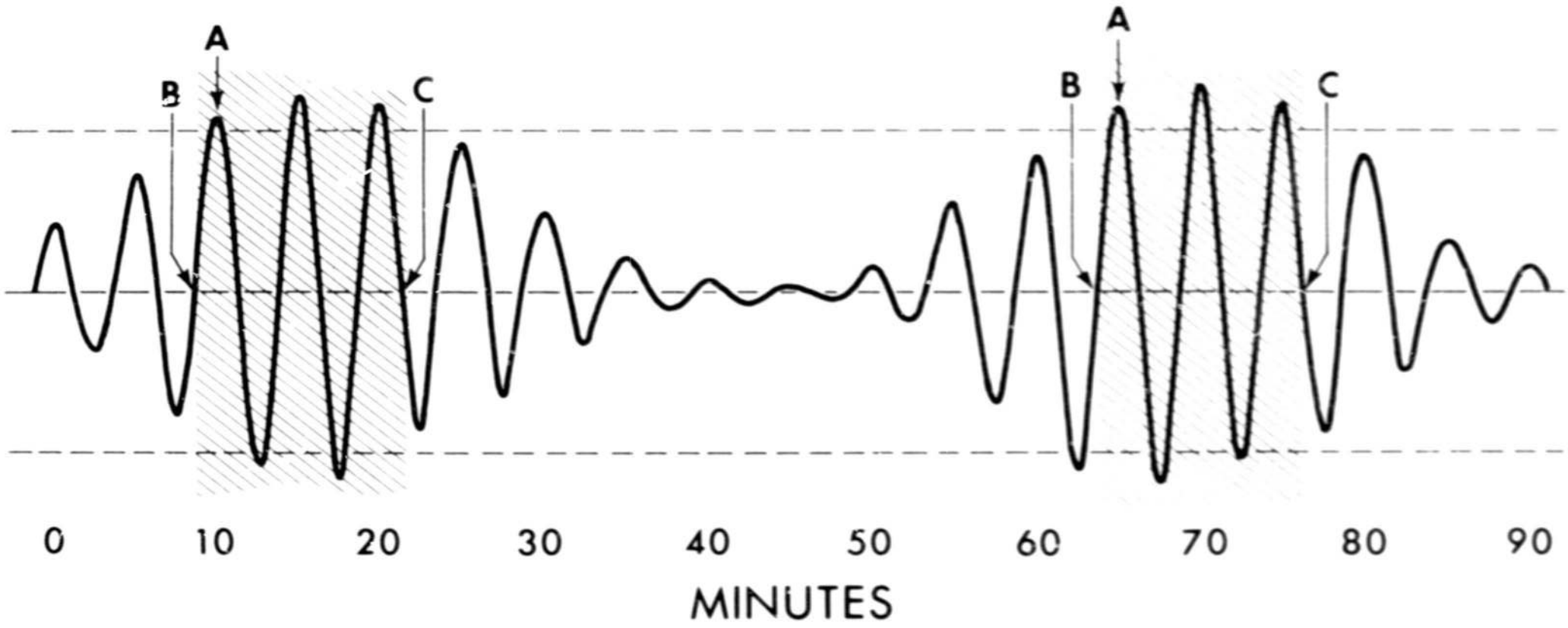


Figure 1

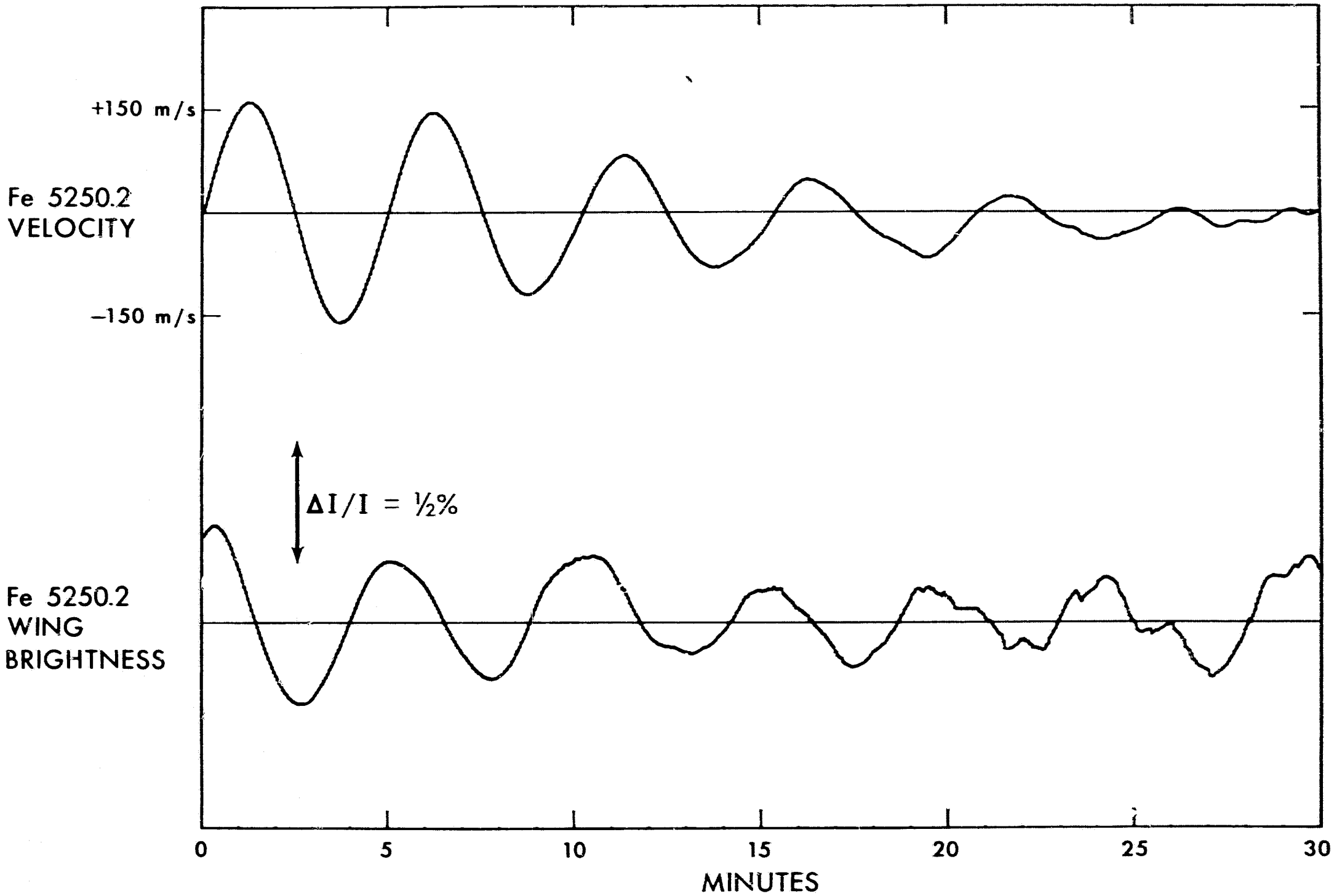
+150 m/s
Fe 5250.2
VELOCITY
−150 m/s
ΔI/I = ½%
Fe 5250.2
WING
BRIGHTNESS
0
5
10
15
20
25
30
MINUTES

Figure 2

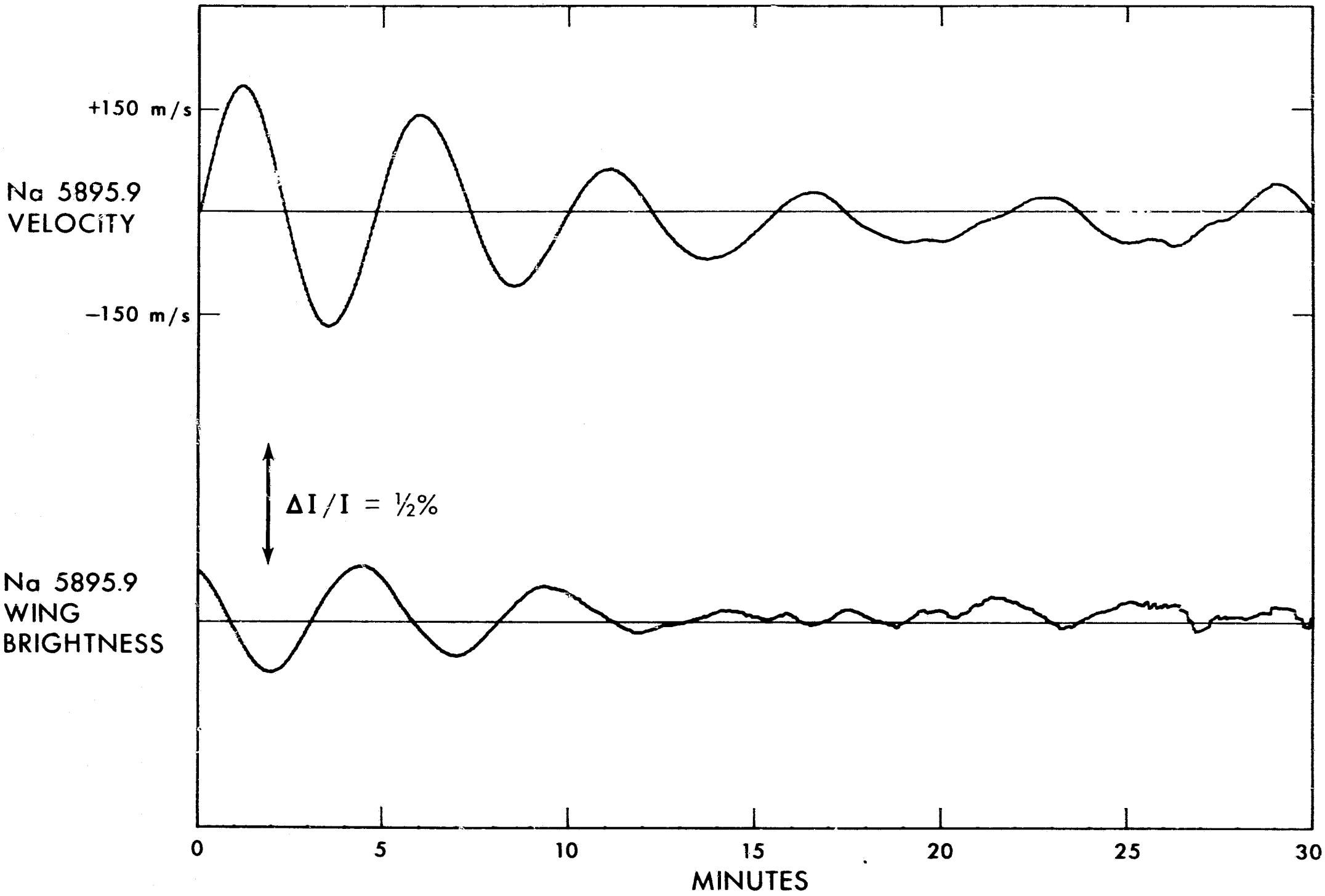
+150 m/s
Na 5895.9
VELOCITY
−150 m/s
ΔI/I = ½%
Na 5895.9
WING
BRIGHTNESS
0
5
10
15
20
25
30
MINUTES

Figure 3

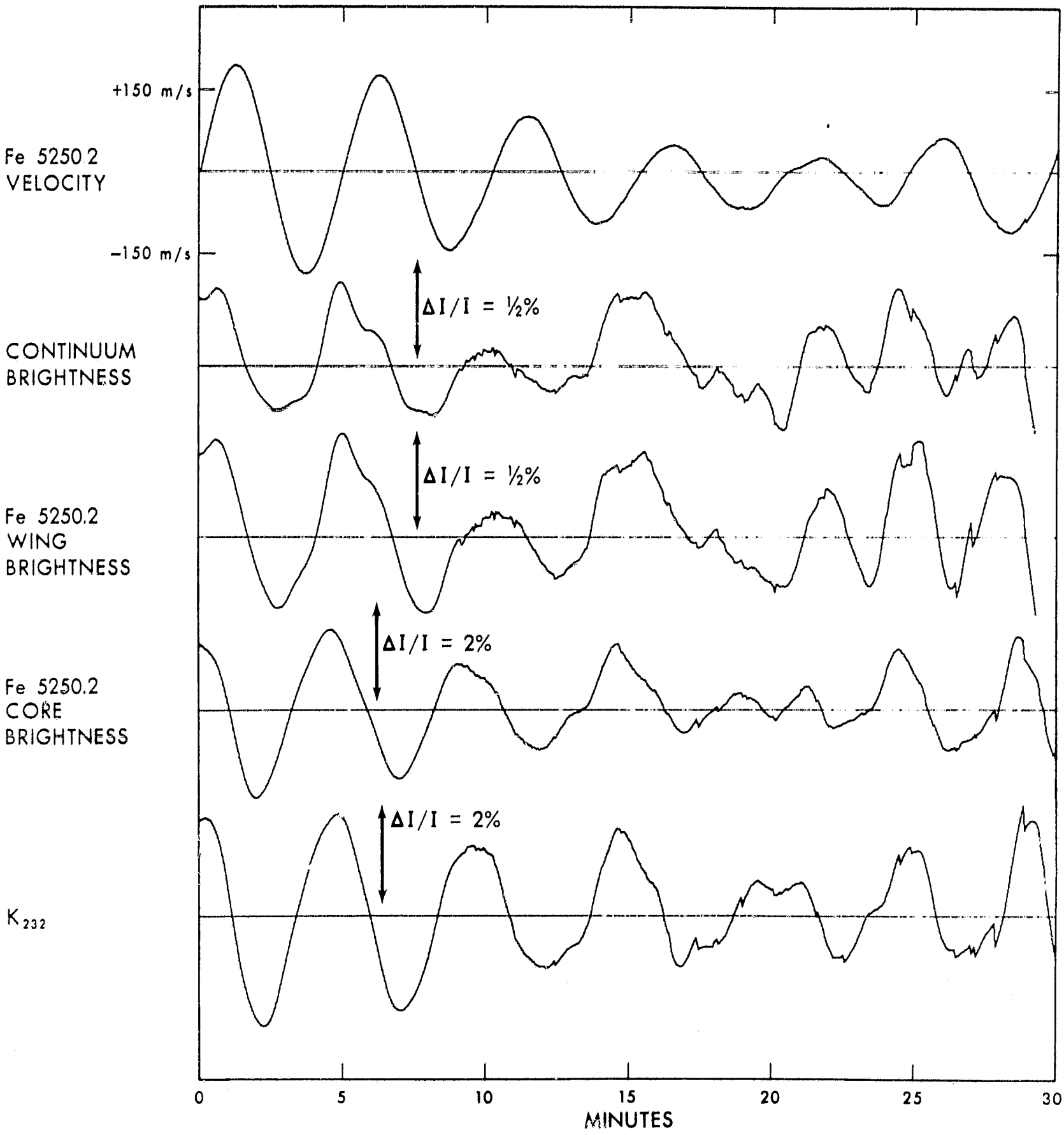
+150 m/s
Fe 5250.2
VELOCITY
−150 m/s
ΔI/Ī = ½%
CONTINUUM
BRIGHTNESS
Fe 5250.2
WING
BRIGHTNESS
ΔI/I = 2%
Fe 5250.2
CORE
BRIGHTNESS
ΔI/I = 2%
K232
0
5
10
15
20
25
30
MINUTES

Figure 4

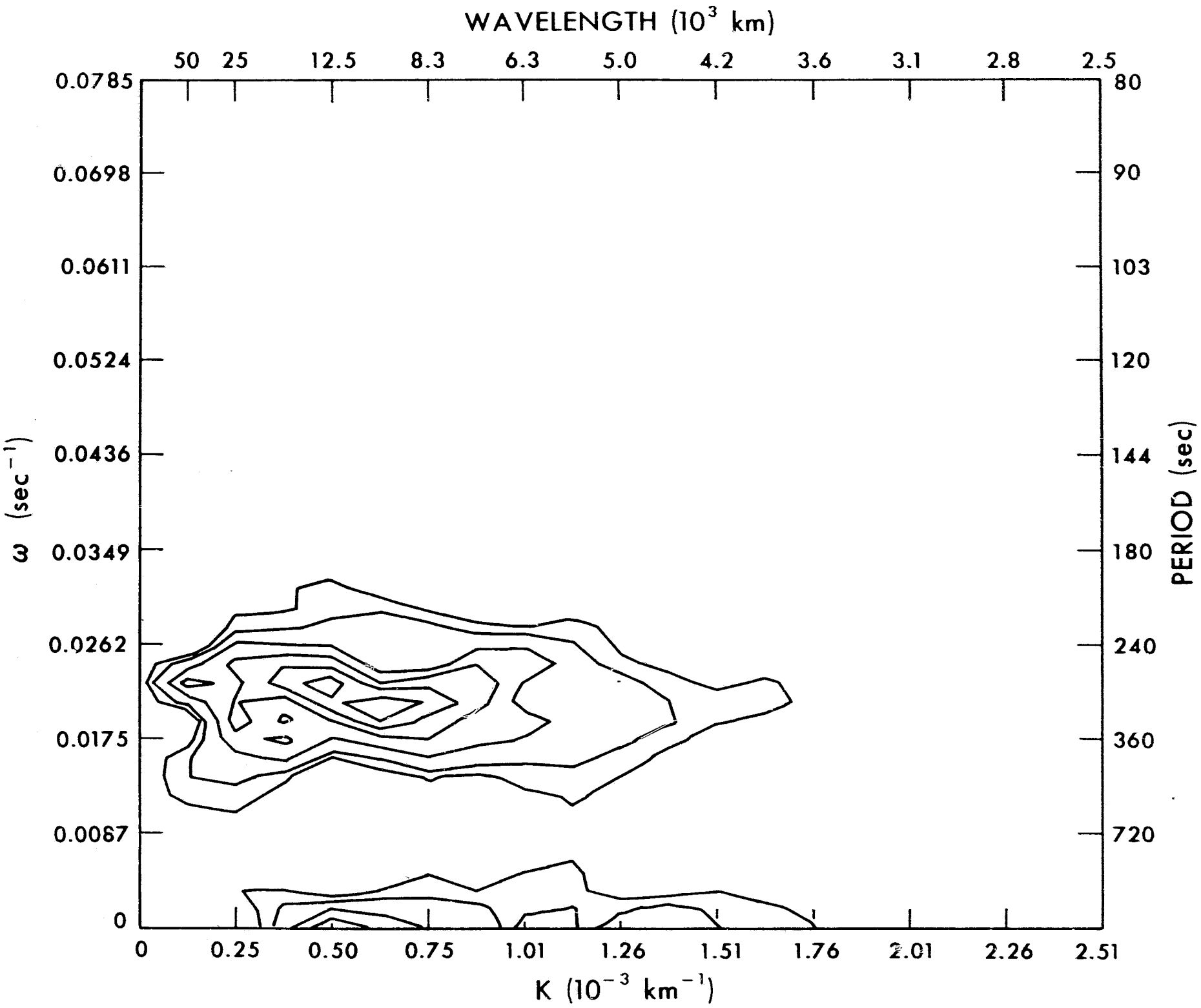
WAVELENGTH ($10^3$ km)
50 25 12.5 8.3 6.3 5.0 4.2 3.6 3.1 2.8 2.5
0.0785
0.0698
0.0611
0.0524
0.0436
0.0349
0.0262
0.0175
0.0087
0
ω (sec$^{-1}$)
80
90
103
120
144
180
240
360
720
PERIOD (sec)
0 0.25 0.50 0.75 1.01 1.26 1.51 1.76 2.01 2.26 2.51
K ($10^{-3}$ km$^{-1}$)

Figure 5

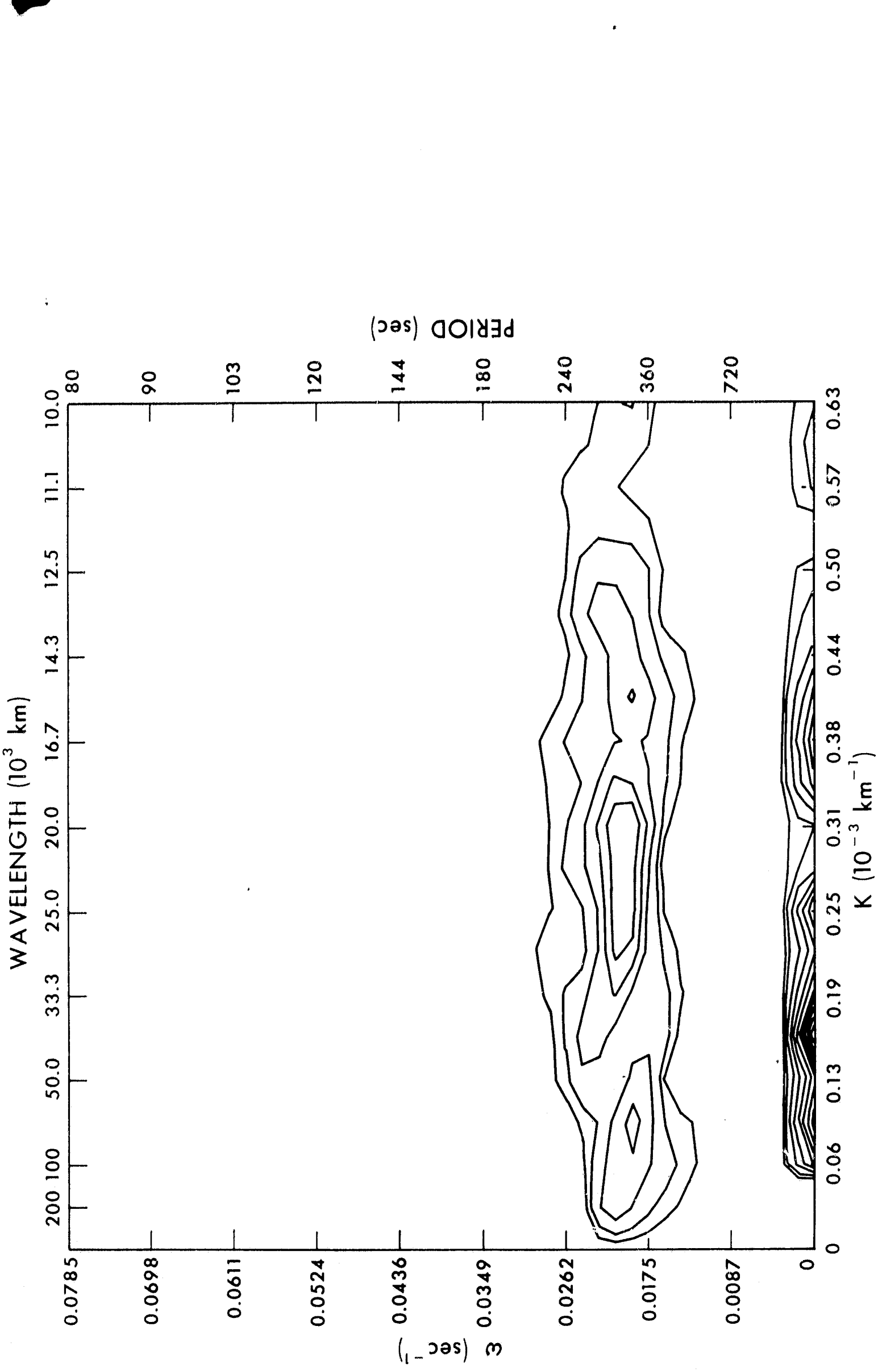
PERIOD (sec)
80
90
103
120
144
180
240
360
720
WAVELENGTH ($10^3$ km)
200 100
50.0
33.3
25.0
20.0
16.7
14.3
12.5
11.1
10.0
ε (sec$^{-1}$)
0.0785
0.0698
0.0611
0.0524
0.0436
0.0349
0.0262
0.0175
0.0087
0
K ($10^{-3}$ km$^{-1}$)
0
0.06
0.13
0.19
0.25
0.31
0.38
0.44
0.50
0.57
0.63

Figure 6

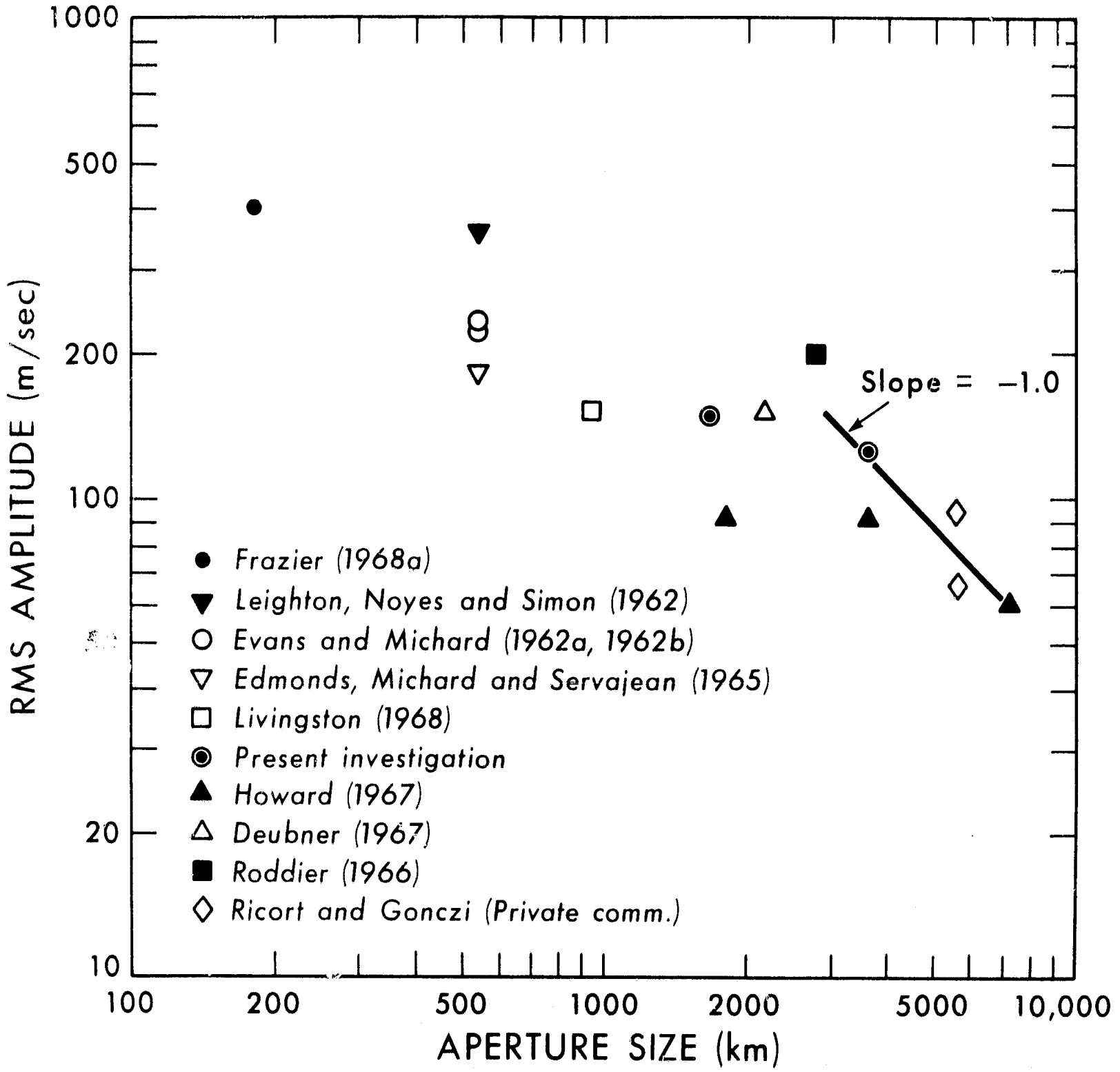
1000
500
200
100
20
10
RMS AMPLITUDE (m/sec)
100
200
500
1000
2000
5000
10,000
APERTURE SIZE (km)
Slope = −1.0
Frazier (1968a)
Leighton, Noyes and Simon (1962)
Evans and Michard (1962a, 1962b)
Edmonds, Michard and Servajean (1965)
Livingston (1968)
Present investigation
Howard (1967)
Deubner (1967)
Roddier (1966)
Ricort and Gonczi (Private comm.)

Figure 7

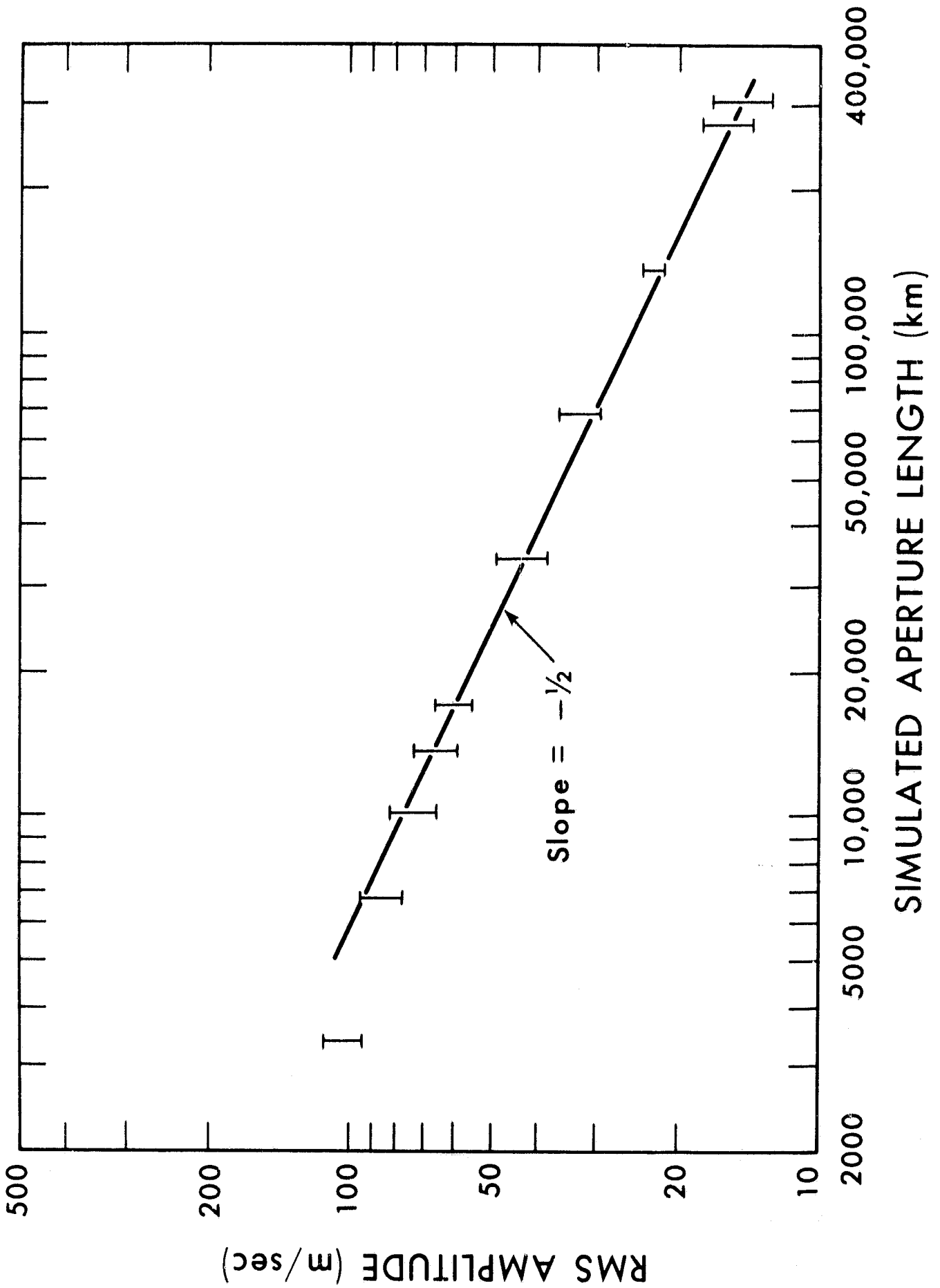
RMS AMPLITUDE (m/sec)
500
200
100
50
20
10
2000
5000
10,000
20,000
50,000
100,000
400,000
SIMULATED APERTURE LENGTH (km)
Slope = −½

Figure 8

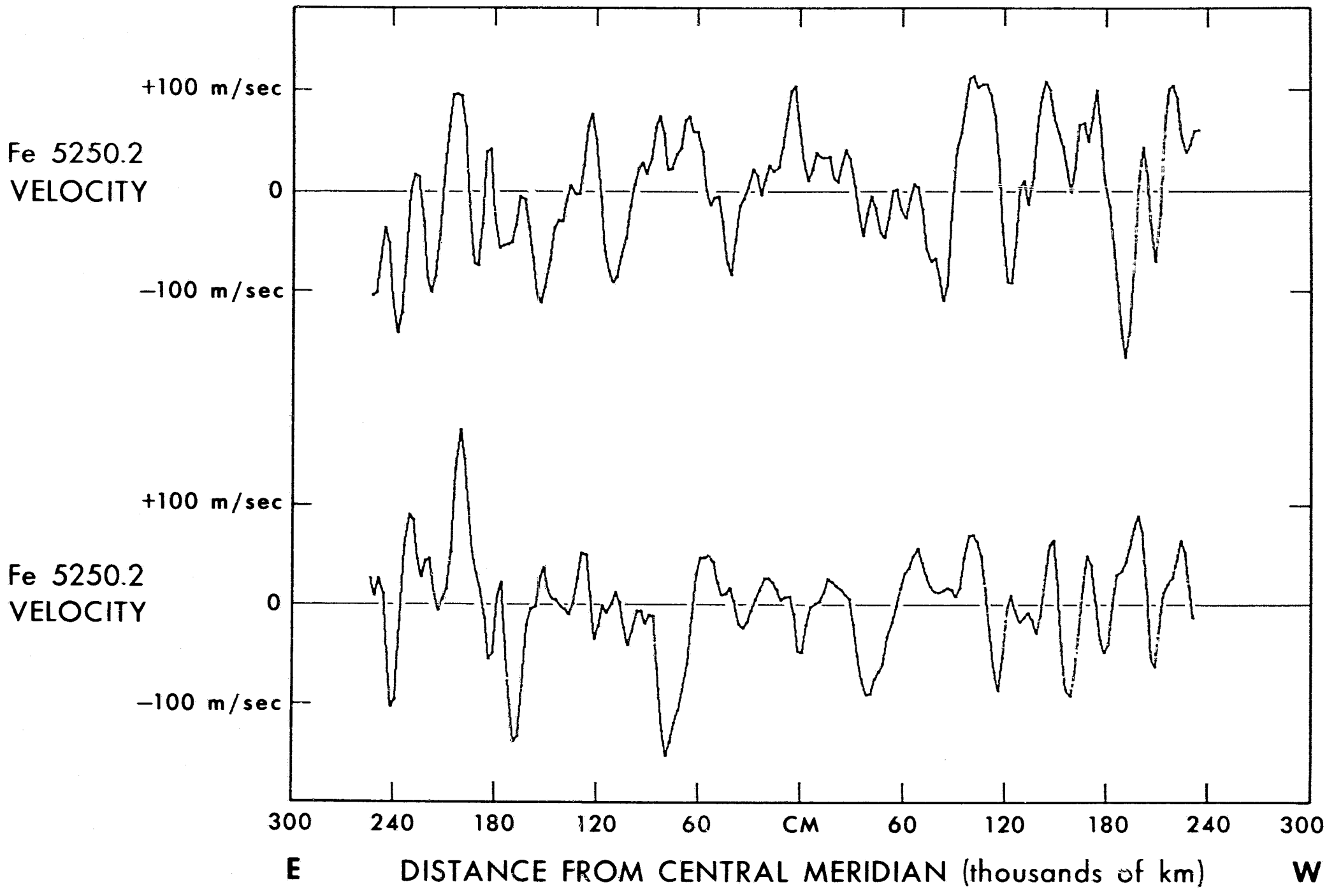
+100 m/sec
Fe 5250.2
VELOCITY
0
−100 m/sec
+100 m/sec
Fe 5250.2
VELOCITY
0
−100 m/sec
300
240
180
120
60
CM
60
120
180
240
300
E
DISTANCE FROM CENTRAL MERIDIAN (thousands of km)
W

Figure 9

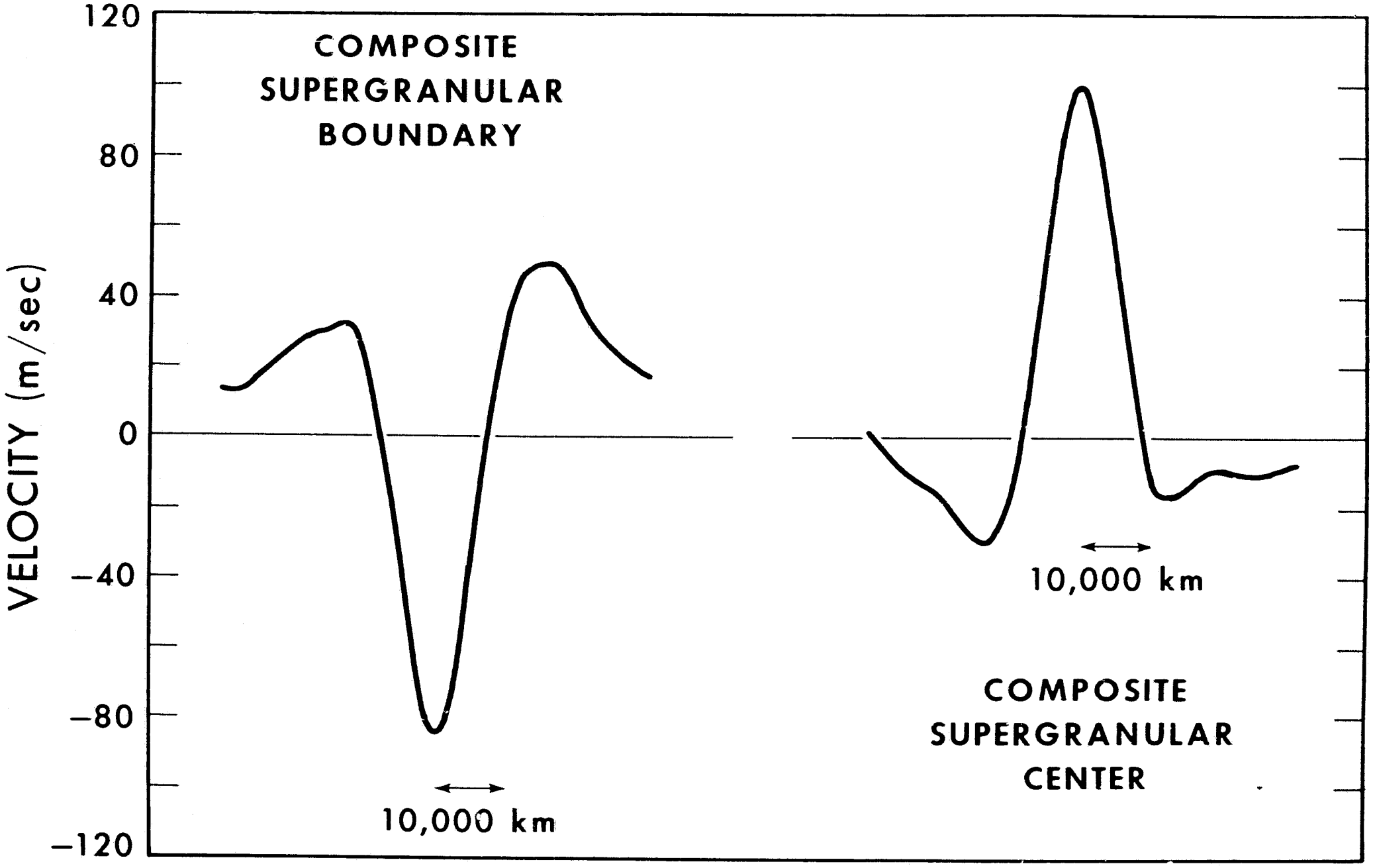
COMPOSITE
SUPERGRANULAR
BOUNDARY
120
80
40
0
−40
−80
−120
VELOCITY (m/sec)
10,000 km
10,000 km
COMPOSITE
SUPERGRANULAR
CENTER

Figure 10

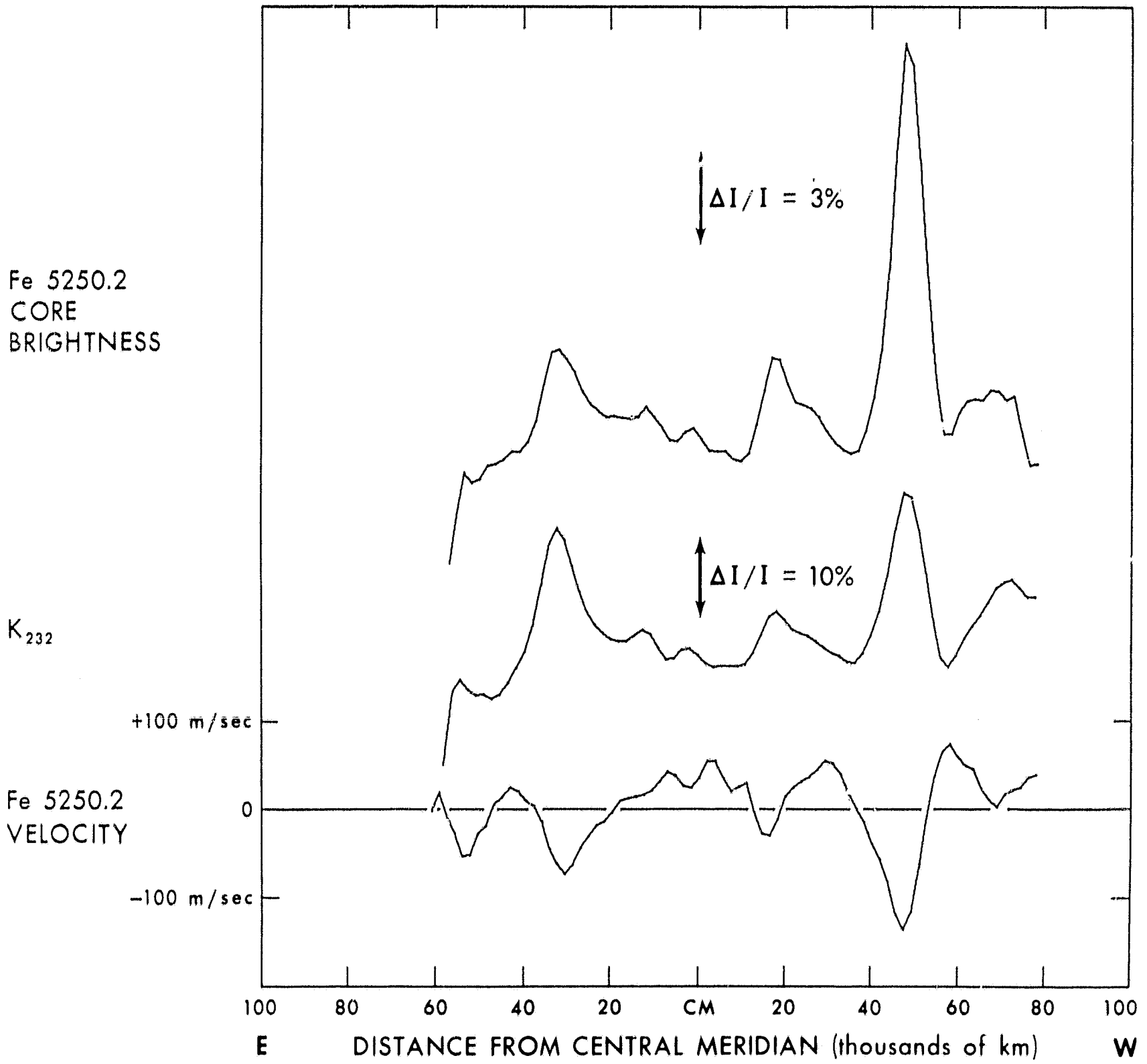
ΔI/I = 3%
ΔI/I = 10%
Fe 5250.2
CORE
BRIGHTNESS
K232
+100 m/sec
0
−100 m/sec
Fe 5250.2
VELOCITY
100
80
60
40
20
CM
20
40
60
80
100
E
DISTANCE FROM CENTRAL MERIDIAN (thousands of km)
W

Figure 11

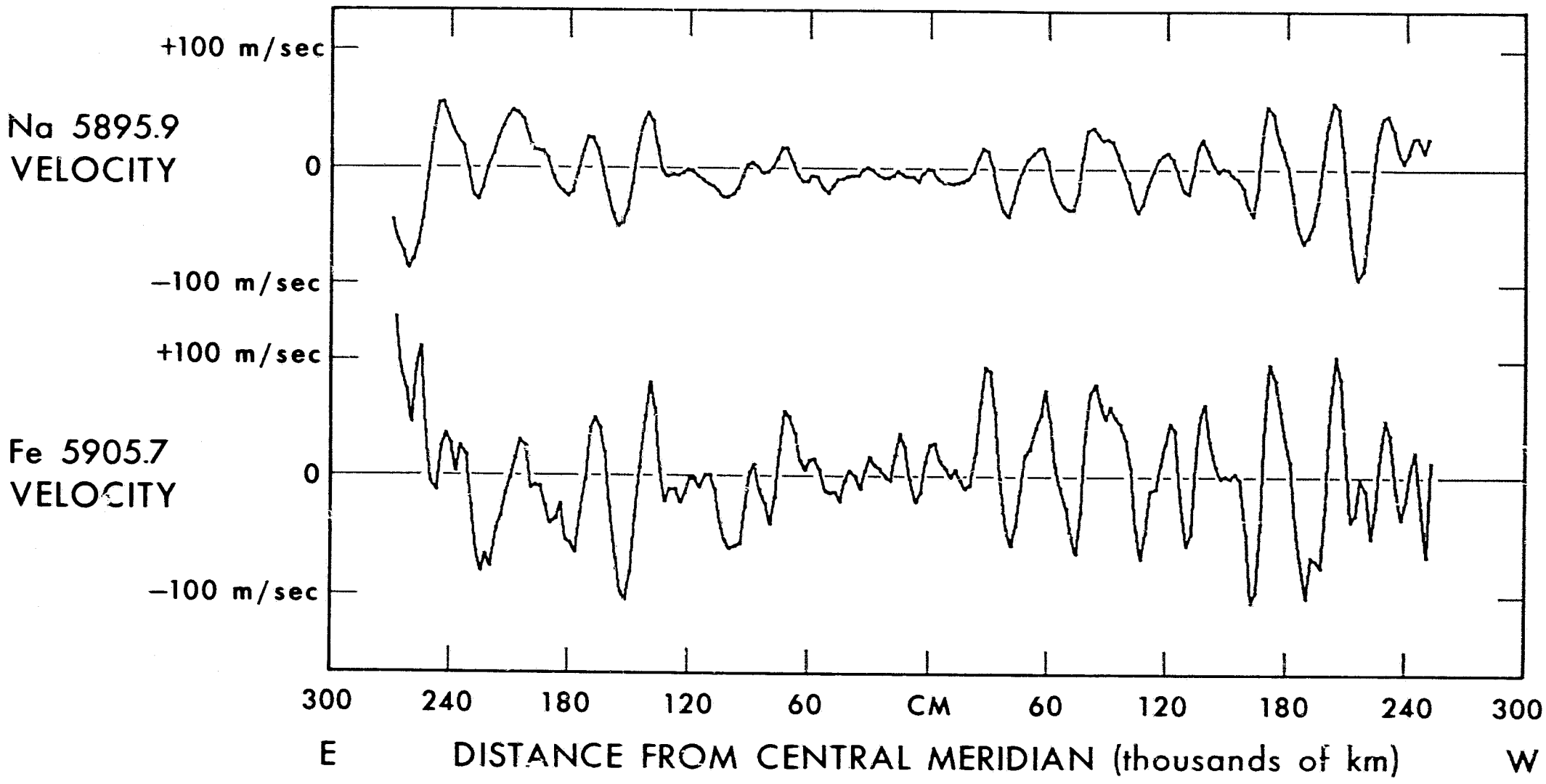
+100 m/sec
Na 5895.9
VELOCITY
0
−100 m/sec
+100 m/sec
Fe 5905.7
VELOCITY
0
−100 m/sec
300
240
180
120
60
CM
60
120
180
240
300
E
DISTANCE FROM CENTRAL MERIDIAN (thousands of km)
W

Figure 12

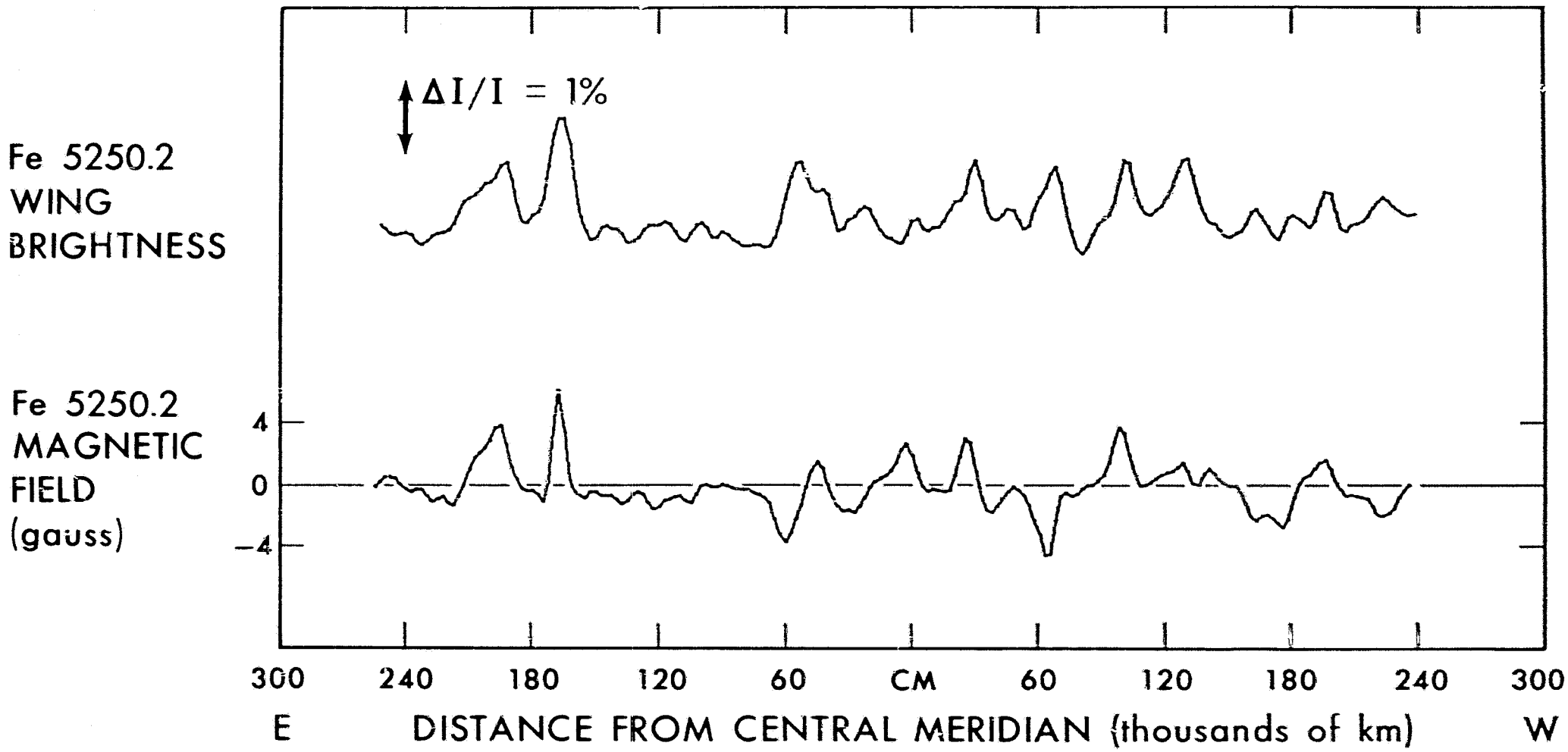
Fe 5250.2
WING
BRIGHTNESS
ΔI/I = 1%
Fe 5250.2
MAGNETIC
FIELD
(gauss)
4
0
−4
300
240
180
120
60
CM
60
120
180
240
300
E
DISTANCE FROM CENTRAL MERIDIAN (thousands of km)
W

Figure 13

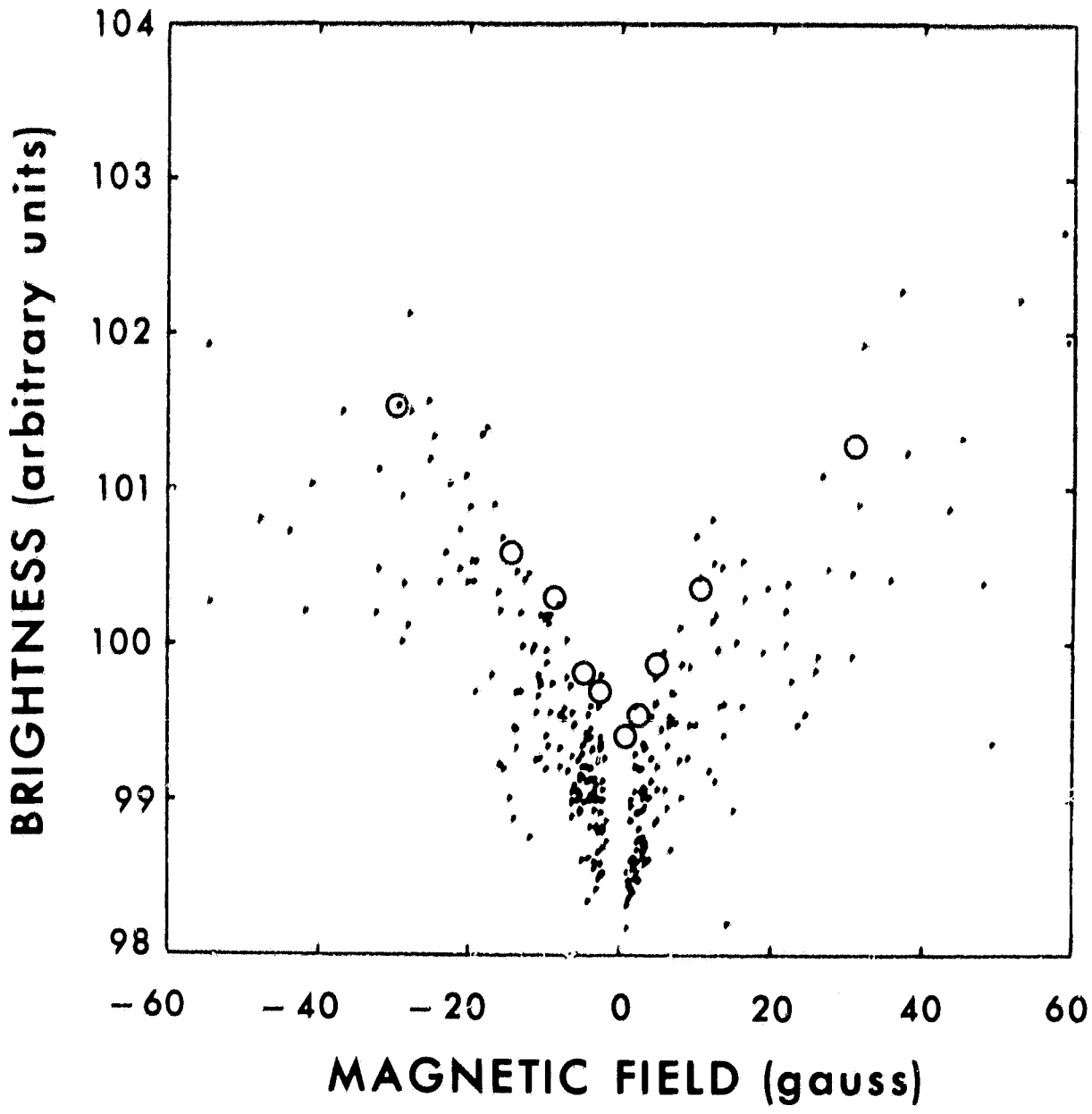
104
103
102
101
100
99
98
BRIGHTNESS (arbitrary units)
−60
−40
−20
0
20
40
60
MAGNETIC FIELD (gauss)

Figure 14